Structural Chemistry (2026) 37:1281–1300
https://doi.org/10.1007/s11224-025-02625-0

RESEARCH

Nicotinamide complexes of metal(II) furan-2-carboxylates: synthesis, determination of crystal structures, Hirshfeld surface analysis, and *in vitro* and *in silico* evaluation of inhibitory properties on CA I, CA II, AChE, BChE, and GR enzymes

Merve Nar[1] · Murat Senturk[2] · Afşin Ahmet Kaya[3] · Füreya Elif Öztürkkan[4] · Elif Çelenk Kaya[3] · Ertan Şahin[5]

Received: 1 August 2025 / Accepted: 15 September 2025 / Published online: 24 September 2025
© The Author(s), under exclusive licence to Springer Science+Business Media, LLC, part of Springer Nature 2025

Abstract

In this study, nicotinamide complexes of Cu^{2+}, Co^{2+}, and Zn^{2+} furan-2-carboxylates were synthesized, and the crystal structures of the complexes were characterized by single crystal X-ray diffraction. The chemical composition and functional groups of the complexes were confirmed using elemental analysis, Fourier transform infrared spectroscopy (FT-IR), ultraviolet–visible region (UV–Vis) spectroscopy, and mass spectrometry (MS). Hirshfeld surface analysis detailed the intermolecular interactions present in the crystal structures of the complexes. The complexes feature a central six-coordinate ion (Cu^{2+}, Co^{2+}, or Zn^{2+}) located on an inversion center, which is bonded to two N atoms from nicotinamide and four O atoms from water molecules. There is a furan 2-carboxylate anion that is not coordinated with metal atoms but links to complex structures via hydrogen bonds. Within the scope of biochemical studies, the inhibitory effects of the synthesized complexes on acetylcholinesterase (AChE), butyrylcholinesterase (BChE), carbonic anhydrase I and II (hCA I, hCA II), and glutathione reductase (GR) enzymes were investigated by spectrophotometric methods. It was determined that the complexes, especially Complex 2, exhibited strong enzyme inhibition properties. Molecular docking analyses revealed the binding tendencies and binding energies of the complexes to the active sites of the enzymes. Complex 2 has a high binding affinity with AChE, BChE, hCA I, hCA II, and GR enzymes, and these bindings were supported by hydrogen bonds and π-π interactions. ADMET predictions showed that the complexes have toxicologically safe profiles despite their pharmacokinetic limitations, such as low gastrointestinal absorption and inability to cross the blood–brain barrier. It was determined that the risks of hepatotoxicity, carcinogenicity, immunotoxicity, and mutagenicity were low. As a result, these metal complexes are evaluated as potential therapeutic agents in the treatment of diseases such as Alzheimer's disease, glaucoma, epilepsy, malaria, and cancer. The data obtained in this study emphasize the biological activities and pharmacological potential of the complexes, and it is recommended that they be supported by future *in vivo* studies.

Keywords Nicotinamide · Furan-2-carboxylate · X-ray crystallography · Enzyme inhibitors · Molecular docking

✉ Afşin Ahmet Kaya
afsinahmet.kaya@omu.edu.tr

✉ Füreya Elif Öztürkkan
fozturkkan36@gmail.com

Merve Nar
evrem36@hotmail.com

Murat Senturk
senturkm36@gmail.com

Elif Çelenk Kaya
elif.celenkkaya@omu.edu.tr

Ertan Şahin
ertan@atauni.edu.tr

[1] Gümüshane Vocatıonal School, Gümüşhane University, 29100 Gümüşhane, Türkiye

[2] Department of Basic Sciences of Pharmacy, Faculty of Pharmacy, Agri Ibrahim Cecen University, Ağrı, Türkiye

[3] Department of Property Protection and Safety, Havza Vocatıonal School, Ondokuz Mayıs University, Samsun, Türkiye

[4] Department of Chemical Engineering, Faculty of Engineering and Architecture, Kafkas University, Kars, Türkiye

[5] Department of Chemistry, Faculty of Science, Ataturk University, Erzurum, Türkiye

Introduction

Metal–organic complexes (MOCs) have attracted significant attention in medicinal and pharmaceutical research due to their structural diversity and potential biological applications. These complexes, formed through coordination bonds between metal ions and organic ligands, exhibit unique physicochemical properties, making them promising candidates for enzyme inhibition, antimicrobial, anticancer, and neuroprotective applications [1, 2]. Transition metal complexes, in particular, are widely studied for their ability to interact with biological macromolecules, influencing key biochemical pathways and offering new strategies for drug development [3]. Among the biologically relevant ligands, nicotinamide (NA)—a derivative of vitamin B3—plays a crucial role in cellular metabolism, particularly as a precursor to nicotinamide adenine dinucleotide (NAD^+), which is essential for redox reactions [4]. Nicotinamide-based metal complexes have been explored for their potential in treating neurodegenerative disorders, metabolic diseases, and oxidative stress-related conditions due to their ability to modulate enzymatic activity and improve bioavailability [5, 6]. Coordination of NA with metal ions can significantly alter its pharmacological profile, leading to enhanced enzyme inhibition and therapeutic efficacy [7]. Similarly, furan-2-carboxylates, a class of heterocyclic carboxylate ligands, are of great interest due to their biological relevance and ability to form stable metal complexes. These ligands possess electron-rich furan rings and carboxylate functionalities, facilitating strong interactions with metal centers and biological targets [8]. Furan-2-carboxylate-based metal complexes have demonstrated various pharmacological properties, including antimicrobial, anti-inflammatory, and enzyme-inhibitory activities [9, 10].

Alzheimer's disease (AD) is a prevalent and widespread form of neurodegenerative illness that impacts millions of people around the world. This type of dementia is characterized by memory, cognitive, and behavioral problems that typically manifest after the age of 65 [2, 11, 12]. Its symptoms progress slowly and may be mistaken for other mental disorders, making it difficult to diagnose. Additionally, the progression of AD is unpredictable, and there is currently no definitive cure [13]. More than 36 million individuals worldwide are impacted by this disease, and unfortunately, the number of individuals suffering from AD is growing each day, with no definitive cure available [14]. At present, AD has no definite and complete cure. Drug therapies currently available can alleviate the symptoms of the disease and decelerate its progression [3]. Enzyme inhibition of cholinesterases, secretases, and monoamine oxidase has been a focus for treating AD [5, 6, 9, 15, 16]. Lately, much research has been dedicated to exploring the potential of cholinesterase inhibitors (ChEI's). The present class of drugs categorized as cholinesterase inhibitors, namely, neostigmine, tacrine, donepezil, and rivastigmine, has been given the green light by the FDA to be used for mild to moderate AD treatment. These drugs have demonstrated efficacy in easing certain symptoms for a limited duration and regulating problematic behavior [3, 12–15]. It was established that these medications come with certain adverse effects and could potentially interact with other drugs [17]. Moreover, the long-term effectiveness of these drugs is limited. An ideal acetylcholinesterase (AChE) inhibitor would need to be both influential and well-tolerated in varying stages of AD. It should also exhibit efficacy in treating other forms of dementia, such as Parkinson's disease. The creation of new ChEI's with minimal side effects and reduced drug interactions is of great significance for the treatment of this condition [12].

Metalloenzyme family carbonic anhydrase (CA) is responsible for the swift conversion of CO_2 to HCO_3^- and a proton. CA isoforms are present in diverse tissues, playing crucial roles in numerous biological processes, including but not limited to CO_2 and ion transport, acid–base balance, lipogenesis, respiration, bone resorption, gluconeogenesis, ureagenesis, and electrolyte secretion [1, 18–21]. Several CA isozymes that play a role in these processes are significant therapeutic targets, and their inhibition or activation could hold promise for treating various disorders, including but not limited to glaucoma, edema, cancer, obesity, and osteoporosis [1, 18–22].

Glutathione reductase (GR) is an indispensable enzyme within the cellular milieu, fulfilling a myriad of crucial functions. These functions encompass gene regulation, maintenance of elevated levels of reduced glutathione (GSH) in comparison to its oxidized form (GSSG), intracellular signal transduction, neutralization of detrimental free radicals, and reactive oxygen species, as well as preservation of the redox equilibrium of intracellular constituents. Under normal physiological circumstances, glutathione predominantly exists in its reduced state (GSH); however, in the face of oxidative stress, a swift conversion to its oxidized form (GSSG) occurs, as this conversion is essential for safeguarding cellular integrity and its various constituents. Nevertheless, the indispensable activity of GR is realized as it facilitates the conversion of GSSG back to GSH through the utilization of NADPH, thereby ensuring the maintenance of an intracellular GSH/GSSG ratio surpassing 99% [4, 23]. The indispensable significance of GSH in numerous cellular processes renders the levels of GSH and the ratio of GSH to GSSG as pivotal factors in an array of human diseases, encompassing, yet not limited to, cancer, cardiovascular diseases, diabetes, AIDS, and AD. Additionally, GSH assumes a crucial role

in the detoxification of hemoglobin, while an elevation in intracellular GSH has been associated with the development of chloroquine resistance. Moreover, compounds that inhibit GR have been identified to possess noteworthy properties as antimalarial and anticancer agents [8, 23, 24].

Heterocyclic metal complexes have garnered significant attention in medicinal chemistry due to their potential biological activities, particularly as antibacterial agents and in the treatment of various diseases. Recent studies illustrate the synthesis and characterization of novel metal-based compounds derived from Schiff bases, such as phenylenediamine and triazole derivatives, which exhibit considerable antibacterial efficacy. The interaction of these ligands with transition metals like copper and zinc not only enhances their chemical stability but also improves their biological performance by facilitating more efficient binding to biological targets. In addition, the structural properties of these complexes can be tuned by adjusting their metal content and ligand frameworks, leading to a diverse array of compounds with tailored pharmacological properties. As a result, heterocyclic metal complexes are positioned as promising candidates in the development of new therapeutic agents, reflecting an amalgamation of synthetic chemistry and biological applications [25–28].

Our objective in this research was to create three innovative compounds containing copper (II), cobalt (II), and zinc (II) furan-2-carboxylates combined with nicotinamide (NA). These compounds could potentially serve as effective therapeutic agents for various medical conditions such as AD, glaucoma, cancer, and more. Three complexes of Cu^{2+}, Co^{2+}, and Zn^{2+} furan-2-carboxylates were synthesized using nicotinamide as a co-ligand. To explore how various metal ions impact inhibition properties, we synthesized three distinct complexes by combining nicotinamide and furan-2-carboxylate. We proceeded to assess the therapeutic potential of the newly synthesized complex molecules by analyzing their inhibitory effects against various enzymes, including AChE, BChE, GR, hCA I, and hCA II enzymes. We discovered that the complexes exhibited hCA I, II, and GR inhibitory properties, which have not been previously reported in the literature. Furthermore, this is the first investigation into the inhibitory properties of these newly synthesized complexes against the aforementioned enzymes.

Experimental section

Materials and methods

Nicotinamide, furan-2-carboxylic acid, sodium bicarbonate, copper (II) sulfate pentahydrate, cobalt (II) hexahydrate, and zinc (II) chloride monohydrate were purchased from Sigma-Aldrich and used without any pre-purification. Melting point determination of synthesized complexes was done with the Gallenkamp brand melting point determination device. C, H, and N elemental analyses were performed with LECO CHNS-932 (Michigan, USA). Infrared spectra were recorded with solid samples in an FT-IR spectrometer, 4000–400 cm^{-1} range, Perkin Elmer Frontier™ spectrometer with ATR detector. UV–VIS measurements were recorded with Perkin Elmer Lambda 35 model Ultraviolet–Visible (UV–VIS) Spectrometer device. Mass spectra were obtained with Thermo-Finnigan mass analyzer (San Jose, USA) and Varian 320-MS (TQ Mass Spectrometer) device.

Synthesis

The synthesis scheme of Complexes 1–3 is given in Fig. S1.

Synthesis of tetraaquabis(pyridine-3-carboxamide-κN) copper(II) furan-2-carboxylate (Complex 1)

Furan 2-carboxylic acid (1 g, 8.92 mmol) was reacted with a solution of sodium bicarbonate (0.74 g, 8.92 mmol) in purified water at boiling temperature to obtain sodium furan-2-carboxylate. The mixing process was continued until the CO_2 gas formed during the reaction was completely removed from the environment. The resulting product was cooled to room temperature. In a separate flask, the solution of copper (II) sulfate pentahydrate salt (1.11 g, 4.46 mmol) in distilled water (50 mL) was mixed with the solution of nicotinamide (1.08 g, 8.92 mmol) in distilled water, and the resulting mixture was mixed with the sodium furan-2-carboxylate solution we obtained earlier. Tetraaquabis(pyridine-3-carboxamide-κ*N*)copper(II) furan-2-carboxylate complex was obtained by reaction with the obtained compound and was crystallized in pure water at room temperature. The crystals formed were filtered and dried in a vacuum in the presence of P_2O_5 at room temperature [29].

Melting point: 254–256 °C. IR (CH_2Cl_2, cm^{-1}): 3308, 3144, 3053, 1685, 1631, 1582, 1535, 1472, 1428, 1364, 1390, 1227, 1191, 1137, 1121, 1065, 1007, 1017, 942, 931, 881, 789, 761, 697, 672, 652, 610. Elemental analysis: calculated $C_{22}H_{26}N_4O_{12}Cu$: C 43.89, H 4.35, N 9.31; Found: C 43.65, H 4.65, N 9.61. MS: m/z 602 [M] +.

Synthesis of tetraaquabis(pyridine-3-carboxamide-κN) cobalt(II) furan-2-carboxylate (Complex 2)

Furan 2-carboxylic acid (1 g, 8.92 mmol) was reacted with a solution of sodium bicarbonate (0.74 g, 8.92 mmol) in purified water at boiling temperature to obtain sodium furan-2-carboxylate. The mixing process was continued until the CO_2 gas formed during the reaction was completely removed from the environment. The resulting product was cooled to room temperature. In a separate flask, the solution of cobalt

(II) chloride hexahydrate salt (1.06 g, 4.46 mmol) in purified water (50 mL) was mixed with the solution of nicotinamide (1.08 g, 8.92 mmol) in distilled water, and the resulting mixture was mixed with the sodium furan-2-carboxylate solution we obtained earlier. Tetraaquabis(pyridine-3-carboxamide-κ*N*)copper(II) furan-2-carboxylate complex was obtained by reaction with the obtained compound, which was crystallized in pure water at room temperature. The crystals formed were filtered and dried in a vacuum in the presence of P_2O_5 at room temperature [7].

Melting point: 248–250 °C. IR (CH_2Cl_2, cm^{-1}): 3295, 3148, 3055, 1686, 1632, 1582, 1541, 1472, 1426, 1389, 1362, 1226, 1192, 1157, 1139, 1119, 1075, 1057, 1017, 1004, 931, 882, 835, 788, 760, 699, 654, 643, 611. Elemental analysis: calculated $C_{22}H_{26}N_4O_{12}Co$: C 44.22, H 4.39, N 9.38; found: C 44.31, H 4.51, N 9.27. MS: m/z 597 [M + 1] +.

Synthesis of tetraaquabis(pyridine-3-carboxamide-κN) zinc(II) furan-2-carboxylate (Complex 3)

Furan 2-carboxylic acid (1 g, 8.92 mmol) was reacted with a solution of sodium bicarbonate (0.74 g, 8.92 mmol) in purified water at boiling temperature to obtain sodium furan-2-carboxylate. The mixing process was continued until the CO_2 gas formed during the reaction was completely removed from the environment. The resulting product was cooled to room temperature. In a separate flask, the solution of zinc (II) chloride monohydrate salt (0.68 g, 4.46 mmol) in purified water (50 mL) was mixed with the solution of nicotinamide (1.08 g, 8.92 mmol) in purified water, and the resulting mixture was mixed with the sodium furan-2-carboxylate solution we obtained earlier. Tetraaquabis(pyridine-3-carboxamide-κ*N*)zinc(II) furan-2-carboxylate complex was obtained by reaction with the obtained compound, which was crystallized in pure water at room temperature. The crystals formed were filtered and dried in a vacuum in the presence of P_2O_5 at room temperature [30].

Melting point: 118–120 °C. IR (CH_2Cl_2, cm^{-1}): 3314, 3147, 3057, 1687, 1637, 1583, 1542, 1473, 1427, 1363, 1390, 1226, 1203, 1192, 1157, 1139, 1119, 1075, 1059, 1017, 1005, 931, 881, 788, 760, 646, 655, 666, 610. Elemental analysis: calculated $C_{22}H_{26}N_4O_{12}Zn$: C 43.76, H 4.34, N 9.28; found: C 43.24, H 4.54, N 9.14. MS: m/z 603 [M] +.

X-ray diffraction analysis

For the structure determination, a single crystal of the complexes 1–3 was used for the data collection on a four-circle Rigaku R-AXIS RAPID-S diffractometer (equipped with a two-dimensional area IP detector). Graphite-monochromated Mo-K_α radiation (λ = 0.71073 Å) and oscillation scans technique with $\Delta w = 5°$ for one image were used for data collection. The lattice parameters were determined by the least-squares methods based on all reflections with $F^2 > 2$ (F^2). Integration of the intensities, correction for Lorentz and polarization effects, and cell refinement were performed using CrystalClear (Rigaku/MSC Inc., 2005) software. The structures were solved by direct methods using SHELXS-97 [31], which allowed for the location of most of the heaviest atoms, with the remaining non-hydrogen atoms being located from different Fourier maps calculated from successive full-matrix least-squares refinement cycles on F^2 using SHELXL-97 [31]. All non-hydrogen atoms were refined using anisotropic displacement parameters. Hydrogens attached to carbons were located at their geometric positions using appropriate HFIX instructions in SHELXL. The aromatic- and methine-H atoms were placed in geometrically idealized positions with C-H = 0.93 and 0.98 Å, respectively, and allowed to ride on their parent atoms, with $U_{iso}(H) = 1.2U_{eq}(C)$ for aromatic- and methine-H atoms. The final difference Fourier maps showed no peaks of chemical significance. The crystallographic data and structural refinement parameters are given in Table 1.

The crystallographic data have been deposited at the Cambridge Crystallographic Data Centre, with CCDC numbers 2433917 (Complex 1), 2433918 (Complex 2), and 2433916 (Complex 3), which can be obtained via www.ccdc.cam.ac.uk/conts/retrieving.html or from the Cambridge Crystallographic Data Centre, 12 Union Road, Cambridge CB21EZ, UK; fax: (+44) 1223-336-033; or deposit@ccdc.cam.ac.uk.

Hirshfeld surface analysis

In recent years, Hirshfeld surface analysis has been extensively used to investigate intermolecular interactions. Hirshfeld surface analysis [32, 33] was performed with the CrystalExplorer 21 program [34] to visualize the intermolecular interactions of the complexes. The crystallographic information file (.cif) of the complexes was used to generate the Hirshfeld surface, d_{norm}, and curvature map and shape index [35] and two-dimensional fingerprint graphs [36]. The normalized contact distance (d_{norm}) is mapped onto the Hirshfeld surface over a fixed color scale, where d_{norm} is defined based on the distances from the surface to the nearest interior (d_i) and exterior (d_e) atoms, relative to their van der Waals radii (r_{iore}^{vdW}):

$$d_{\text{norm}} = \frac{d_i - r_i^{vdW}}{r_i^{vdW}} + \frac{d_e - r_e^{vdW}}{r_e^{vdW}}$$

Negative *d*_norm values (red spots) indicate contacts shorter than the sum of van der Waals radii, while positive values (blue regions) correspond to longer contacts. The

Table 1 Crystal data, data collection, and structure refinement details of complexes 1–3

Empirical formula	$C_{12}H_{20}CuN_4O_6$ •2($C_5H_3O_3$).H_2O (Complex 1)	$C_{12}H_{20}CoN_4O_6$ • 2($C_5H_3O_3$) (Complex 2)	$C_{12}H_{20}ZnN_4O_6$ • 2($C_5H_3O_3$) (Complex 3)
Formula weight	602.02	597.40	603.86
Temperature (K)	293 (2)	293 (2)	293 (2)
Wavelength (Å)	0.71073	0.71073	0.71073
Crystal system	Triclinic	Triclinic	Triclinic
Space group	*P*−1	*P*−1	*P*−1
Unit cell dimensions (Å, °)	*a* = 7.0348(5) *alpha* = 85.951(3) *b* = 7.1653(5) *Beta* = 76.903(3) *c* = 14.1285(10) *Gamma* = 62.196(2)	*a* = 6.9700(9) *alpha* = 83.733(5) *b* = 7.0268(8) *Beta* = 77.666(4) *c* = 14.4291(18) *Gamma* = 64.595(4)	*a* = 6.9755(3) *alpha* = 84.068(3) *b* = 7.0431(3) *Beta* = 77.631(1) *c* = 14.3436(5) *Gamma* = 64.296(2)
Volume ($Å^3$)	613.05(8)	623.50(13)	620.18(4)
Z	1	1	1
Density (calculated) (g/cm^3)	1.631	1.591	1.617
Absorption coefficient (mm^{-1})	0.965	0.761	1.064
F(000)	311	309	312
Theta range for data collection	2.9 to 28.8°	3.3 to 28.3°	3.2 to 26.4°
Index ranges	$-9 \le h \le 9, -9 \le k \le 9, -19 \le l \le 19$	$-9 \le h \le 9, -9 \le k \le 9, -19 \le l \le 19$	$-8 \le h \le 8, -8 \le k \le 8, -17 \le l \le 17$
Reflections collected	24,766	19,650	17,869
Independent reflections	3191 [*R*(int) = 0.068]	3084 [*R*(int) = 0.027]	2551 [*R*(int) = 0.043]
Data completeness (%)	99.7	98.9	1.00
Refinement method	Full-matrix least-squares on F^2	Full-matrix least-squares on F^2	Full-matrix least-squares on F^2
Data/restraints/parameters	2712/0/183	2966/0/183	2288/0/183
Goodness-of-fit on F^2	1.054	1.101	1.064
Final *R* indices [I > 2σ(I)]	*R*1 = 0.034 w*R*2 = 0.0471	*R*1 = 0.023 w*R*2 = 0.025	*R*1 = 0.027 w*R*2 = 0.034
R indices (all data)	*R*1 = 0.077 w*R*2 = 0.2083	*R*1 = 0.0667 w*R*2 = 0.0667	*R*1 = 0.064 w*R*2 = 0.067
Largest diff. peak and hole ($eÅ^3$)	0.31 and −0.59	0.36 and −0.27	0.29 and −0.30

procedure follows the standard methodology reported by Spackman and Jayatilaka [35].

In vitro and in silico enzyme inhibition studies

The used materials and equipment, AChE, BChE, CA I, CA II, and GR inhibition assay, were supplied as supplementary information.

Molecular docking has become an indispensable computational tool in structural and medicinal chemistry, as it provides valuable insights into the binding affinity, orientation, and interaction patterns between small molecules and their biological targets [37, 38]. Molecular docking of the complexes into the AChE [39], BChE [40], CA I [41] CA II [10], and glutathione reductase [42] enzymes was performed using AutoDock Vina [43]. The crystal structure of the acetylcholinesterase (PDB ID: 1ACJ), butyrylcholinesterase (PDB ID: 4BDS), carbonic anhydrase I (PDB ID: 1AZM), carbonic anhydrase II (PDB ID: 3HS4), and glutathione reductase (PDB ID: 1XAN) enzymes was downloaded from the RCS Protein Data Bank (http://www.rcsb.org/pdb). The Lamarckian Genetic Algorithm (LGA) technique was used for all calculations for the ligand-target flexible docking. To provide the PDB format for the complex, to prepare the target from the structures of proteins, and to visualize the docking analysis, we used Discovery Studio 2021 Client [44] The cif files of the complexes were used to prepare the pdb extension files of the complexes, and they were converted to pdbqt files via AutoDock Vina software.

ADMET predictions

Molecular docking of the complexes into the acetylcholinesterase makes it is possible to identify the pharmacokinetic and toxicokinetic features of drug candidate molecules, avoiding the need for additional trials and increasing success rates. The features that a therapeutic molecule must possess are described by the absorption, distribution, metabolism, excretion, and toxicity (ADMET) criteria. The Swiss ADME [45] online database was used to determine the complexes'

values for absorption, distribution, metabolism, and excretion. The ProTox-II [46] and admetSAR [47] online databases were used to calculate toxicology estimates.

Results and discussion

Single crystal structure analysis

The structures of Cu^{2+}, Co^{2+}, and Zn^{2+} complexes; tetraaquabis(pyridine-3-carboxamide-κ*N*)copper(II) furan-2-carboxylate hydrate (Complex 1), tetraaquabis(pyridine-3-carboxamide-κ*N*)cobalt(II) furan-2-carboxylate (Complex 2), and tetraaquabis(pyridine-3-carboxamide-κ*N*)zinc(II) furan-2-carboxylate (Complex 3) were determined by single crystal analysis (Figs. 2, 3, and 4). All structures are crystallized in the triclinic P-1 space group and have similar coordination, and the lattice parameters are very close to each other. Again, in all structures, there is a furan 2-carboxylic acid anion that is not coordinated with the metal atoms but is connected to the complex structures by hydrogen bonds. The complexes contain a six-coordinate Cu^{2+}, Co^{2+}, and Zn^{2+} ion lying on an inversion center, which is bonded to two nicotinamide N atoms and four aqua O atoms. Intermolecular hydrogen-bonding interactions are present, linking the Cu^{2+}, Co^{2+}, and Zn^{2+} complex cations and furan 2-carboxylic acid anions in the crystal structure.

In each complex, the metals exhibit a distorted octahedral geometry and are located on a crystallographic center of symmetry with nicotinamide N donors, two aqua O atoms in equatorial positions, and other aqua atoms in axial positions. The metal–ligand bond lengths are N1-Cu = 1.994, O5-Cu = 2.417, O4-Cu = 2.015, N1-Co = 2.130, O2-Co = 2.077, O1-Co = 2.157, N2-Zn = 2.103, O2-Zn = 2.184, and O3-Zn = 2.112 Å (Table 2). The notable difference in the Cu-O5 and Cu-N1/CuO4 bond lengths leads to an elongation of the coordination octahedron, which is associated with the Jahn–Teller effect that is commonly observed for Cu^{2+} complexes. As for the intermolecular interactions, effective N–H•••O, O–H•••O, and C-H•••O hydrogen bonds occur between the aqua ligand and the oxygen of furan 2-carboxylic anion, and again between anionic furan 2-carboxylic acid and nicotinamide and coordinated nicotinamides (Table 3). The coordination polyhedron of the metal atom in Complexes 1–3 is typical for such complexes. The average bond lengths of Co–O and Co–N in the tetraaquabis(nicotinamide-κ*N1*)cobalt(II) bis(2-fluorobenzoate) complex were reported as 2.109 Å and 2.145 Å [48]. The average bond lengths of Cu–O and Cu–N in the tetraaquabis(3-pyridinecarboxamide-κ*N*)-copper(II) bis(2,4,6-trinitrophenolate) complex were reported as 2.165 Å and 2.034 Å [49]. These bond distances are consistent with the bond distances determined in our synthesized cobalt and copper complexes. Although there is no zinc complex with a similar structure containing nicotinamide, the tetraaquabis(isonicotinamide-κN1)zinc bis(3-hydroxybenzoate) tetrahydrate complex has been reported [50]. In this complex, it is seen that the Zn–O (2.108 Å) and Zn-N (2.117 Å) bond lengths have bond distances close to the zinc complex in our study. N–H•••O and O–H•••O hydrogen bonds were also determined in these complexes. There are π-π stacking interactions between the delocalized π-electrons of the heterocyclic pyridine and furan rings. For example, in the Co(II) complex, the distance between ring centroids is in the range of 3.5506(3)–4.1324(3) Å with the slipping angle ranges of 19.0–31.3 degrees. However, vdW interactions contribute to the formation of a stable structure. Since the unit cell lattices are the same, polyhedral images of the molecules Cu(II), Co(II), and Zn(II) complexes are given in Figs. 1, 2, and 3 along the *a*, *b*, and *c*-axes, respectively.

Table 2 Geometric parameters of the complexes 1–3 (Å, °)

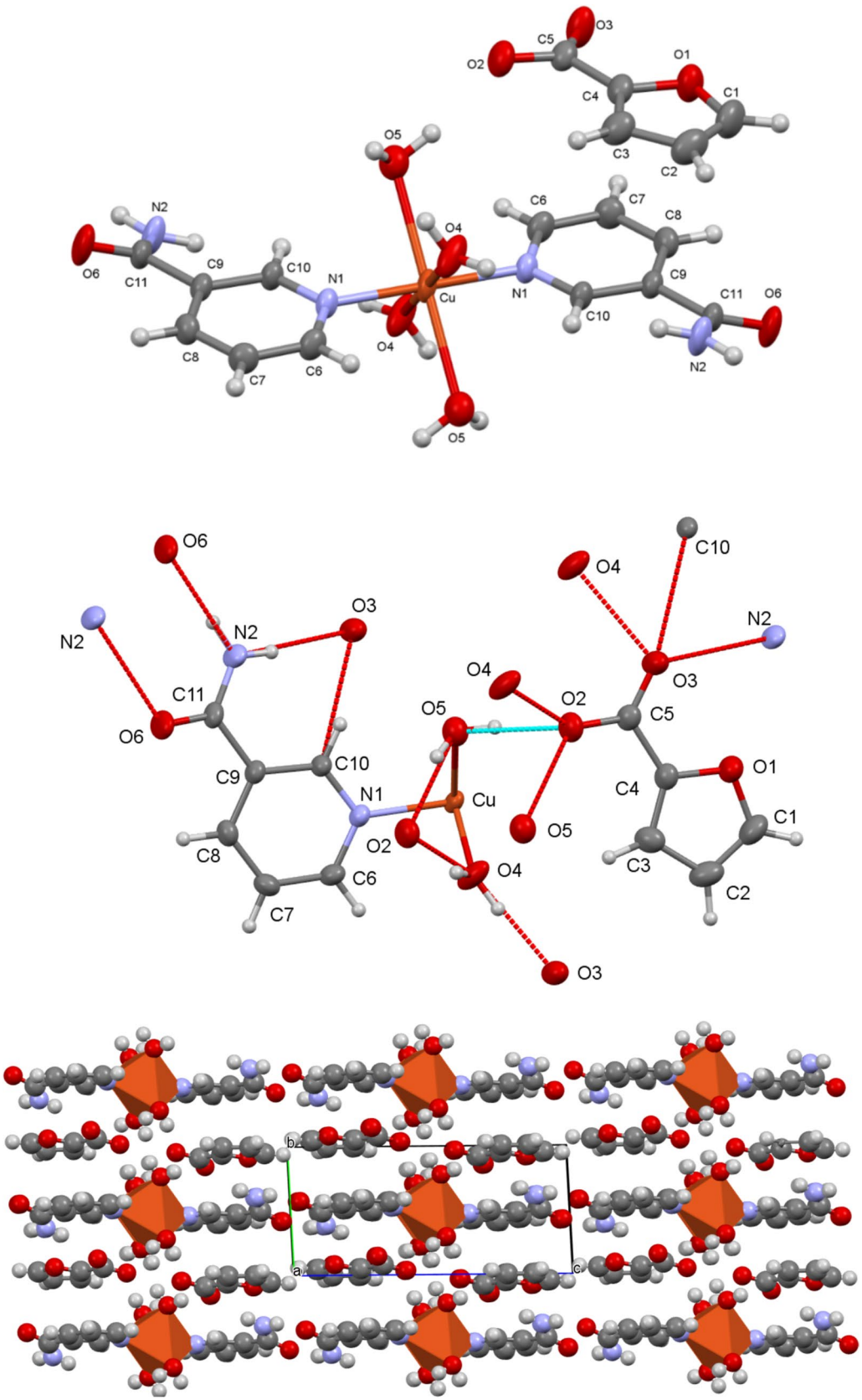
Complex 1			
Cu-N1	1.994 (3)	N1-C10	1.339 (3)
Cu-O5	2.417 (3)	N1- C6	1.342 (3)
Cu-O4	2.015 (3)	N2-C11	1.327 (3)
O4-Cu-O5	86.5	O5-Cu-N1	88.1
O5-Cu-O4-N1	88.2	O4-Cu-N1-C6	−51.6
Complex 2			
Co-N1	2.130 (3)	N1-C5	1.343 (3)
Co-O1	2.157 (3)	N1 –C1	1.344 (3)
Co-O2	2.077 (2)	N2-C6	1.331 (3)
O1-Co-O2	87.79	O1-Co-N1	92.98
O2-Co-N1	92.14	O2-Co-N1-C5	42.9
Complex 3			
Zn-N2	2.103 (2)	N2-C5	1.340 (3)
Zn-O3	2.112 (2)	N2-C1	1.338 (3)
Zn-O2	2.184 (2)	N1-C6	1.327 (3)
O2-Zn-O3	92.12	O2-Zn-N2	87.78
O3-Zn-N2	92.07	O3-Zn-N2-C5	−43.4

Hirshfeld surface analysis

Hirshfeld surface analysis is an analysis that presents intermolecular interactions in the form of visual graphics with different colors and color intensities. When the d_{norm} maps of the complexes are examined, interactions with shorter distances than the Van der Waals radius, i.e., close contacts, are seen as red surfaces, and interactions with longer distances than the Van der Waals radius, i.e., longer contacts, are seen as blue surfaces. On the d_{norm} maps, the white surfaces represent the distances equal to the sum of the Van der Waals radii (Fig. 4a–f). D_{norm} maps on the 3D Hirshfeld surfaces of the synthesized complexes were determined in the range

Table 3 Hydrogen-bond geometry of the complexes 1–3 (Å, °)

D-H···*A*	*D*—H	H···*A*	*D*···*A*	*D*—H···*A*
Complex 1				
N2-H2A···O6^{i}	0.86	2.05	2.892 (2)	165
N2-H2B···O3^{ii}	0.86	2.19	3.040 (2)	170
O4-H4A···O2^{iii}	0.90	1.92	2.759 (2)	155
O4-H4B···O3^{iv}	0.86	1.81	2.658 (2)	171
O5-H5A···O2^{v}	0.89	1.96	2.822 (2)	165
O5-H5B···O2^{iii}	0.89	1.94	2.793 (2)	161
Symmetry codes: (i) 1-x,1-y,-z,-z; (ii) 1+x,y,z; (iii) *x,1+y,z*; (iv) −1-x,1-y,1-z; (v) -x,1-y,1-z				
Complex 2				
N2-H2A···O5^{i}	0.86	2.05	2.893 (2)	166
N2-H2B···O3^{ii}	0.86	2.21	3.053 (2)	168
O1-H1A···O4	0.88	1.92	2.786 (2)	165
O1-H1B···O4^{iii}	0.86	1.92	2.760 (2)	160
O2-H2C···O3^{ii}	0.85	1.82	2.674 (2)	174
O2-H2D···O4^{iii}	0.89	1.94	2.777 (2)	154
Symmetry codes: (i) 1-x,1-y,-z; (ii) 1+x,y,z; (ii) *1+x,y,z* ; (iii) -x,-y,1-z				
Complex 3				
N1-H1A···O1^{i}	0.86	2.05	2.888 (2)	166
N1-H1B···O6^{ii}	0.86	2.19	3.035 (2)	168
O2-H2A···O5^{iii}	0.87	1.91	2.749 (2)	164
O2-H2B···O5^{iv}	0.88	1.94	2.788 (2)	162
O3-H3A···O6^{ii}	0.84	1.84	2.682 (2)	174
O3-H3B···O5^{v}	0.92	1.93	2.789 (2)	155
Symmetry codes: (i) 1-x,1-y,-z; (ii) 1+x,y,z; (iii) *x,1+y,z*; (iv) -x,1-y,1-z; (v) -x,-y,1-z				


O3
C5
O2
O1
C4
C1
C3
C2
O5
N2
C6
C7
C8
O4
O6
C11
C9
C10
N1
Cu
N1
C9
C11
O6
C10
C8
O4
N2
C7
C6
O5
O6
N2
O3
N2
C11
O6
C10
C9
N1
Cu
C8
O2
C6
C7
O4
O3
C10
O4
N2
O3
O4
O2
O5
C5
O5
O1
C4
C1
C3
C2
b
a
c

◂**Fig. 1** (top) A view of the molecule Complex 1, with the atom-numbering scheme. Displacement ellipsoids are drawn at the 40% probability level, and H atoms are shown as small spheres of arbitrary radii. (mid.) *H*-bond geometry, symmetry codes are given in Table 3. (bottom) Polyhedral view of the stacked Complex 1 with the unit cell viewed down along the *a*-axis

of −0.7191–1.1707 a.u. (cationic unit) and −0.7197–1.1108 a.u. (anionic unit) (Complex 1), −0.7117–1.1926 a.u. (cationic unit), and −0.7109–1.1729 a.u. (anionic unit) (Complex 2), and −0.7050–1.1731 a.u. (cationic unit), and −0.7056–1.1323 a.u. (anionic unit) (Complex 3) [33].

The adjacent red and blue triangles appearing in the shape indices of the complexes 1–3 (Fig. 5a–f) are due to the C-H…π and π …π interactions of aromatic rings (furan and pyridine) in the structures of the complexes [33].

The large green surfaces seen in the curvature maps of the complexes (Fig. 6a–f) represent a planar surface area. These regions are seen where aromatic rings are found in the structure of the complexes. The flat regions around these rings confirm the existence of π–π stackings. The blue regions represent the curvedness areas.

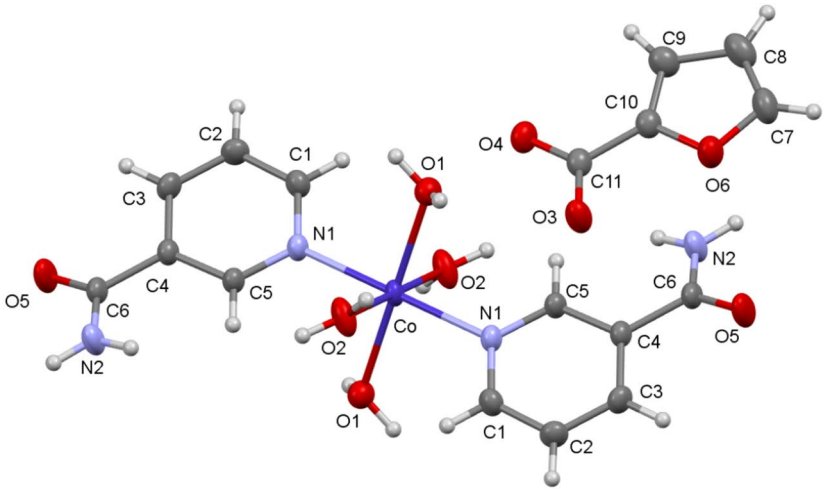
Hirshfeld surface and fingerprint plot analyses demonstrate that the interaction landscape of all three complexes is dominated by H…H and H…O/O…H contacts. In the cationic units, these two contributions account for 73.8% in Complex 1 (H…H 38.9%; H…O/O…H 34.9%), while higher totals are observed in Complex 2 (78.6%) and Complex 3 (78.7%), with H…H at 40.7/40.6% and H…O/O…H at 37.9/38.1%. In the anionic units, the distributions are more consistent: 74.6% for Complex 1 (H…H 31.9%; H…O/O…H 42.7%), 74.1% for Complex 2, and 74.3% for Complex 3 (H…H 32.3/32.6%; H…O/O…H 41.8/41.7%). These values indicate that the hydrate molecule present exclusively in Complex 1 enhances the hydrogen-bonding network particularly around the anionic unit (highest anionic H…O/O…H at 42.7%), accompanied by a concomitant reduction of H…H contacts (lowest anionic H…H at 31.9%). In the cationic unit of Complex 1, the H…O/O…H contribution (34.9%) is about three percentage points lower than in Complex 2 and 3 (37.9–38.1%), with a parallel decrease in H…H, suggesting a redistribution of hydrogen-bonding interactions from the cationic unit towards the anionic unit in the hydrated structure.

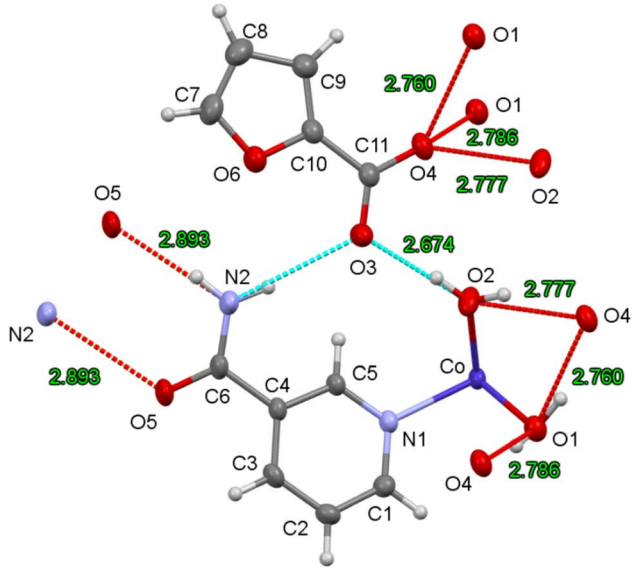
Aromatic-related interactions are well preserved throughout the series. In the cationic units, C…C contacts (π···π stacking) contribute 9.1% in Complex 1 and 8.7% in Complexes 2–3, while H…C/C…H contacts (mostly C–H···π) reach 5.0% in Complex 1 compared to 4.0% in Complexes 2–3. As a result, the combined "π-related" share (C…C + H…C/C…H) is slightly higher in Complex 1 (14.1%) than in the Co and Zn analogues (~ 12.7%). In the anionic units, C…C contributions are identical across all structures (11.3%), while H…C/C…H varies only marginally (5.7% for Complex 1, 5.5% for Complex 2, and 5.3% for Complex 3), confirming the persistence of π–π stacking between aromatic rings and C–H···π contacts across the isostructural series. The C…O/O…C contacts, representing weak polar or edge interactions involving carbonyl oxygens and aromatic carbons, are in the range of 4.4–4.8% in the cationic units, while in the anionic units they are 5.0% for Complex 1 and 5.7% for Complexes 2–3, reflecting a slight (~ 0.7%) reduction in the hydrated structure due to the stronger involvement of water-mediated O–H···O interactions.

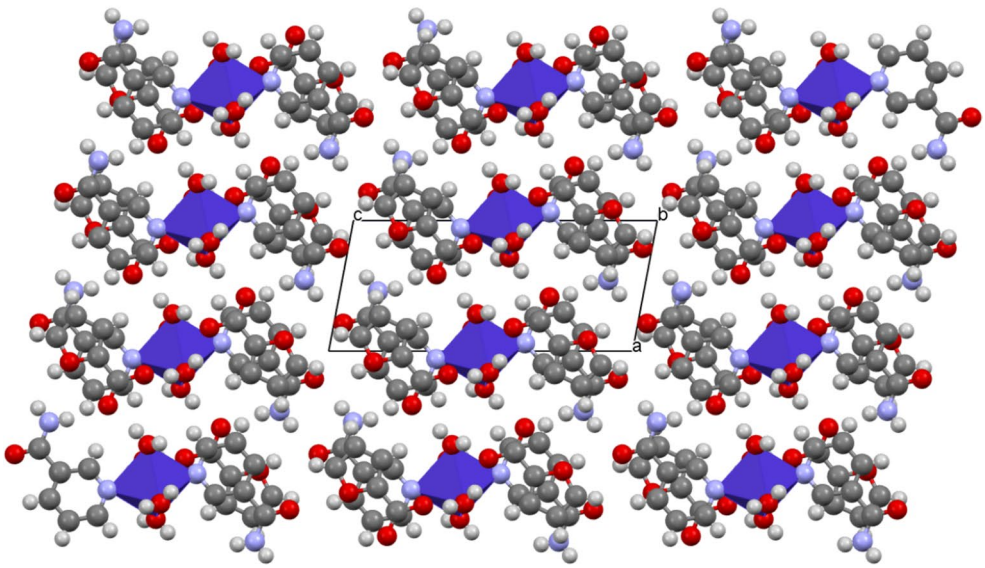
Hydrogen-bond signatures given by H…N/N…H contacts are higher in the cationic unit of Complex 1 (4.0%) compared to Complexes 2–3 (2.7%), while remaining low and similar in the anionic units (1.6–1.8%). Negligible contributions (< 1%) include C…N/N…C (0.6–0.7% in the cationic units; 0.8–0.9% in the anionic units), N…O/O…N (0.2–0.4% overall), and O…O (0.2–0.7%). These minor interactions contribute little to the packing relative to the dominant O–H···O and N–H···O motifs. Metal-centered contacts are detected only in Complex 1, with H…Cu at 0.3% and O…Cu at 1.8%, whereas such interactions are absent in the Co and Zn analogues. Collectively, these results confirm that the three complexes are isostructural and share a common supramolecular profile, with the hydrate in Complex 1 subtly altering the balance of contacts by enhancing anionic H…O/O…H interactions, reducing H…H contributions, and introducing weak Cu-centered contacts that fine-tune the crystal packing. Two-dimensional fingerprint plots for cationic and anionic units are given in Figs. S2–S3 (Complex 1), Figs. S4–S5 (Complex 2), and Figs. S6–S7 (Complex 3). Percentages of intermolecular interactions according to 2D fingerprint graphs of complexes 1–3 are given in Table 4.

Infrared and UV–Vis spectroscopy results

FT-IR spectra of Complex 1–3 are given in Figs. S8–S10. The broad bands in the range of 3600–3200 cm^{-1} are the vibrations of the O–H groups of water molecules. The asymmetric and symmetric NH_2 vibration bands of the amide group of the nicotinamide molecule were also observed at 3300–3100 cm^{-1}. In the IR spectra of the complex compounds synthesized in this study, the specific carboxyl group peak of the acids is not observed. Instead, the presence of v_{asCOO-} and v_{sCOO-} peaks indicates that the protons of the carboxyl groups are lost but do not bond with the metal atom. The asymmetric and symmetric COO- absorption bands of the carboxylic group are observed around 1580 cm^{-1} and 1380 cm^{-1}. Aromatic C-H vibrations were observed at 3053 cm^{-1} (Complex 1), 3055 cm^{-1} (Complex 2), and 3057 cm^{-1} (Complex 3). For complexes 1–3, the carboxamide C = O bands of the nicotinamide molecule were observed


C9
C8
C10
C7
O4
C11
O6
O3
C2
C1
O1
C3
N1
N2
O2
C5
C6
O5
C4
Co
N1
C5
C6
N2
O2
C4
O5
O1
C3
C1
C2


C8
O1
C7
C9
2.760
O1
2.786
C11
O6
C10
O4
2.777
O2
O5
2.893
2.674
O3
N2
O2
2.777
O4
N2
2.893
Co
2.760
C6
C4
C5
O5
N1
O1
C3
O4
2.786
C2
C1


c
b
a

◂**Fig. 2** (top) A view of the molecule Complex 2, with the atom-numbering scheme. Displacement ellipsoids are drawn at the 40% probability level, and H atoms are shown as small spheres of arbitrary radii. (mid.) *H*-bond geometry, symmetry codes are given in Table 3. (bottom) Polyhedral view of the stacked Complex 2 with the unit cell viewed down along the *b*-axis

at 1687 cm^{-1}, 1686 cm^{-1}, and 1687 cm^{-1}, respectively. C-N vibrations of the pyridine ring were observed at 1362 cm^{-1}, 1364 cm^{-1}, and 1363 cm^{-1}. For complexes 1–3, the C-O of furan rings were observed at 1535 cm^{-1}, 1541 cm^{-1}, and 1542 cm^{-1}, respectively. C–O–C vibrations of the furan ring were observed at 1227 cm^{-1}, 1226 cm^{-1}, and 1226 cm^{-1}. The IR data indicate that the furan ring does not participate in coordination within the complexes. The functional groups of the three isostructured complexes were observed in the same regions close to each other in the FT-IR spectra [51].

Unsaturation in the molecule results in UV region absorption. Due to the unsaturated conjugate structures in organic solids, UV–VIS and IR spectroscopy are widely used in qualitative analyses for such compounds.

When the UV–VIS region spectra were examined, the synthesized complexes exhibited maximum absorbance at 263–266 nm. Accordingly, when the energies of the bonds are low, they sometimes absorb low-energy rays. On the other hand, they have higher energies and they absorb shorter wavelengths, that is, higher energy rays. This distinction allows us to analyze. Considering the wavelength range (263–266 nm) exhibited by complexes 1, 2, and 3, it has been determined that they have π-π* and n-π* transitions. This value range is defined as the near UV region. In this way, we can obtain qualitative analysis results as well as quantitative results (Figs. S11–S13 and Table S1).

Biochemical studies

For the purposes of this study, we employed a straightforward one-step method utilizing affinity chromatography to purify hCA I and hCA II [20–22]. AChE, BChE, hCA I, hCA II, and GR enzymes' inhibitory activities with complexes 1–3 were determined by using different spectrophotometric methods. These two cytosolic CA isozymes were assayed by the method described by Verpoorte et al. [52]. Cholinesterase activities were tested by the method described by Ellman et al. [53]. GR activity was tested by the method described by Beutler et al. [54]. In this study, donepezil was used as a reference drug for cholinesterases. Acetazolamide (**AZA**) was used to test CA enzymes. N,N-bis(2-chloroethyl)-N-nitrosourea (**NNS**) was used for GR enzyme. The IC_{50} values obtained for complexes 1–3 are summarized in Table 5. These enzyme K_i values were calculated from Lineweaver–Burk plots and are given in Table 6.

Our group previously conducted a study on the inhibitory effects of Si-Phthalocyanine derivatives on hCA I and hCA II [18]. A different investigation explored the inhibitory potential of certain water-soluble phthalocyanines on the enzymes AChE and BChE [15]. Research conducted on various metal-complexed compounds demonstrated effective inhibition profiles against these five tested enzymes. Consequently, the decision was made to screen newly synthesized metal complexes and their precursors for their inhibitory effects on these enzymes. Compounds (Figs. 1, 2, and 3) with distinct functional groups on the nicotinamide and Furan-2-carboxylate were assessed for their ability to inhibit AChE and BuChE using Ellman's colorimetric assay [53]. The reference compound used in this research was donepezil, a cholinesterase inhibitor available in the market. Furthermore, this study marks the initial investigation into the inhibitory effects of Complexes 1–3 on the esterase activity of hCA I and hCA II. Tables 5 and 6 data reveal the following outcomes of these compounds' inhibitory effects on the enzymes, measured by an esterase assay with 4-nitrophenylacetate (4-NPA) as the substrate:

(i) Complex 1–3 exhibit effective inhibition against the slow cytosolic isozyme hCA I, with K_i values ranging from 98.6 to 222.7 nM. These results are consistent with previous studies, which demonstrate that functional groups such as pyridine on the exterior of phthalocyanine structures can interact with enzymes [12]. In comparison with the specific CA inhibitor acetazolamide (368 nM), it was observed that the structures of the tested compounds exhibited stronger inhibition of hCA I. Among the tested substances, Complex 2 (98.6 nM) was found to be the most potent inhibitor.

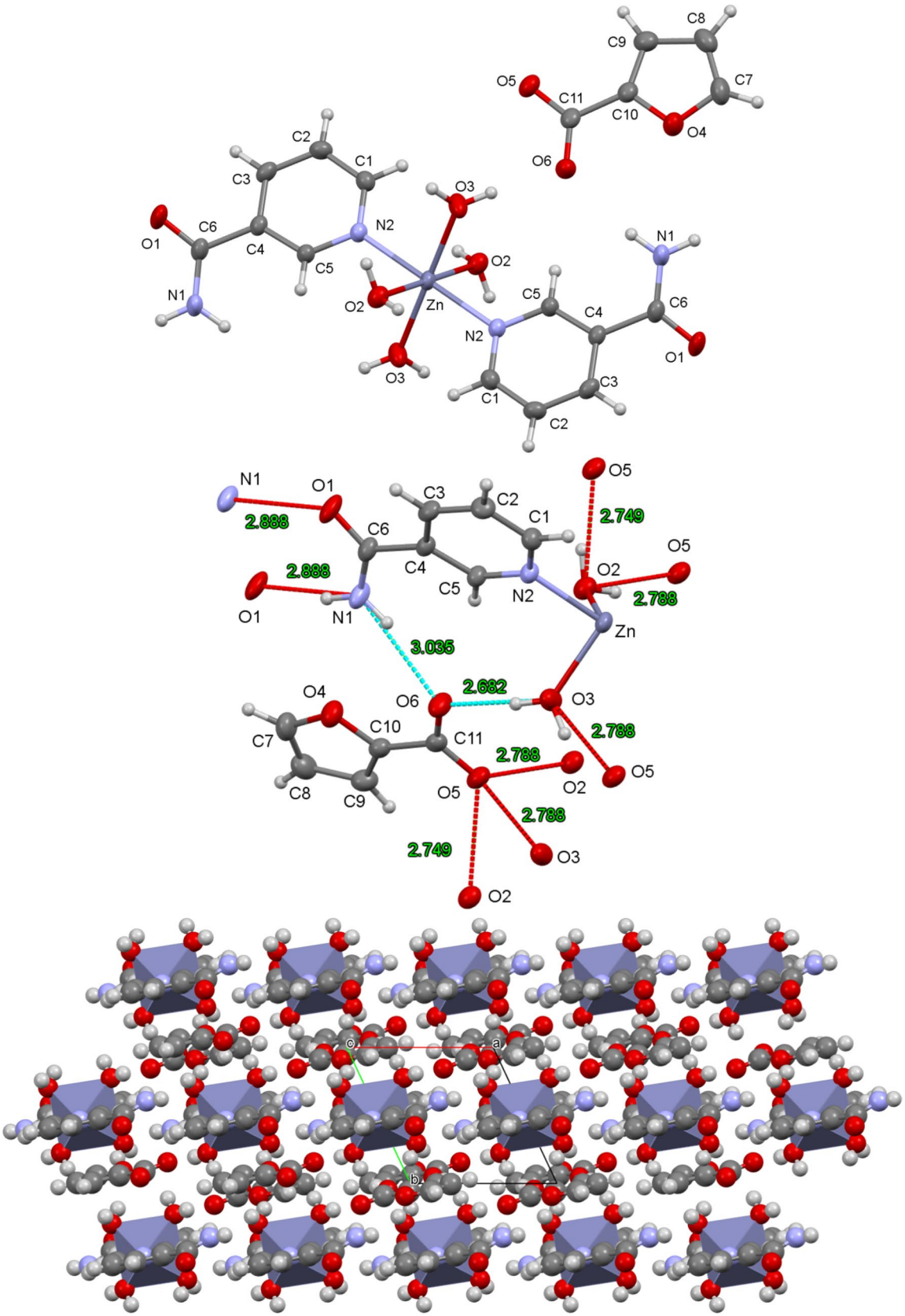
IC_{50}: 50% inhibitory concentration (means ± SD of three experiments) of tested enzymes

Errors within the range of 1–2% were observed in the presented data, as obtained from three distinct assays

(ii) In the assessment of inhibitory activity against the rapid cytosolic isozyme hCA II (Table 6), the tested compounds exhibit superior performance. Of the complexes examined in this study, Complex 3 (195.5 nM) was the least effective inhibitor against hCA II. Complex 2 (K_i 68.0 nM) emerged as the most potent inhibitor of hCA II among this group of derivatives.

(iii) Complex 1–3 acts as a very good inhibitor with K_i values in the range of 7.5—16.6 nM against the GR enzyme, which is the target in the treatment of malaria and cancer. The reason why the inhibition effect is so high is probably because the complex structure of nicotine amide is similar to NADPH, the substrate of this enzyme. The best GR inhibitor in this derivative series was Complex 2 with a K_i of 7.5 nM.

(iv) Complexes 1–3 exhibit significant inhibitory properties against AChE, with K_i values ranging from 151.6


C8
C9
O5
C11
C7
C10
O4
O6
C2
C1
C3
O3
N2
C6
O1
C4
C5
N1
O2
O2
Zn
C5
N1
C4
C6
N2
O1
O3
C3
C1
C2
N1
O1
O5
C3
C2
2.888
C1
2.749
C6
O5
2.888
C4
O2
C5
N2
2.788
O1
N1
Zn
3.035
2.682
O4
O6
O3
C10
2.788
C7
C11
2.788
O5
O2
C8
C9
O5
2.788
O3
2.749
O2
c
a
b

◂**Fig. 3** (top) A view of the molecule Complex 3, with the atom-numbering scheme. Displacement ellipsoids are drawn at the 40% probability level, and H atoms are shown as small spheres of arbitrary radii. (mid.) *H*-bond geometry; symmetry codes are given in Table 3. (bottom) Polyhedral view of the stacked Complex 3 with the unit cell viewed down along the *c*-axis

to 257.4 nM. In this study, Complex 3 emerged as the weakest inhibitor against AChE, while Complex I (K_i value from 151.6 nM) was found to be the most effective AChE inhibitor among the examined complexes. In comparison to the cholinesterase inhibitor donepezil (201.4 nM), it was observed that the structures of these metal complexes displayed more robust inhibition of AChE. Complex 1 was the most effective inhibitor among the tested substances.

(v) Complex 1–3 display potent inhibitory activity against BChE, with K_i values ranging from 234.8 to 425.9 nM. In this study, Complex 3 was identified as the weakest inhibitor against BChE, while Complex I (with a K_i value of 234.8 nM) was found to be the most effective BChE inhibitor among the examined metal complexes. It was observed that the structures of these metal complexes exhibited stronger inhibition of BChE compared to cholinesterase inhibitors such as donepezil (1022.3 nM).

Molecular docking results

Molecular docking studies are carried out to enrich pharmacological data and to provide biological material for bioactivities. It indicates how potential drug candidates interact with target proteins in the active site. Given the encouraging *in vitro* results, it was thought useful to perform molecular docking studies. According to the *in silico* molecular docking data in Table S2, the docking score (binding energy) of all proteins is negative, which indicates that the synthesized complexes 1–3 bind to target proteins. The binding energies of the Complex 1 complex to these enzymes were determined as −9.4, −9.9, −7.2, −8.2, and −7.9 kcal/mol, respectively. The binding energies of Complex 2 to AChE, BChE, CA I, CA II, and GR enzymes were found to be −10.7, −10.1, −8.2, −9.4, and −9.7 kcal/mol, respectively. The binding energies of Complex 3 to these enzymes were determined as −7.5, −9.1, −6.0, −7.7, and −8.4 kcal/mol, respectively. The binding affinity of Complex 1 towards the AChE enzyme is lower than that of the reference drug donepezil and has a value close to BChE. It has been determined that the binding affinity of this complex to other enzymes is higher than the reference drugs. When the binding energy values are examined, it is seen that Complex 2 has the best binding affinity to all proteins compared to both Complex 1 and Complex 3 and reference drugs. In Fig. 7, the interactions of Complex 2 with these tested enzymes are presented. The binding energy of the Complex 3 to CA I and BChE enzymes was found to be lower than their reference drugs (donepezil and acetazolamide, respectively). The binding affinity of this complex to AChE, CA II, and GR enzymes is higher than the reference drugs. The binding affinities of AChE, BChE, CA I, and CA II enzymes were determined as Complex 2 > Complex 1 > Complex 3, and the binding affinity of the complexes to GR was Complex 2 > Complex 3 > Complex 1 during cobalt, copper, and zinc complexes. As seen in Table S1, there are many interactions such as conventional hydrogen bonds, carbon-hydrogen bonds, π-donor hydrogen bonds, π-anion, π-π stacked, π-π T-shaped, amide-π stacked, π-cation, π-alkyl, alkyl, π-sigma, π-sulfur between the target protein and the complexes. The hydrogen bond interactions generated in the structure of both ligands and target proteins by the hydrogen bond donor and acceptor groups contribute greatly to protein–ligand interactions. The hydrogen bond distances between the cobalt complex and asp72, trp84, gly118, ser122, trp432, and gln69, the amino acid residues in the active site of the AChE enzyme, were determined as 2.74, 2.27, 2.70, 2.53, 2.61, and 2.13 Å, respectively. Complex 1 exhibited a hydrogen bond interaction only with the amino acid glu199 ($d = 2.59$ Å) in this active site. Complex 3 forms hydrogen bonds with amino acids tyr334, glu199, and tyr121 in the active site of AChE. The bond lengths were determined as 2.46 Å, 1.83 Å, and 2.44 Å, respectively. Complexes 1–3 form hydrogen bonds with amino acid residues trp82 (2.69 Å), tyr128 (2.38 Å), ser198 (2.28 Å), and his43 (2.17 Å); tyr128 (2.30 Å), ser198 (2.15 Å), his438 (2.37 Å), asp70 (2.16 Å), and glu197 (1.90 Å); and gly117 (2.65 Å), ser198 (2.28 Å), his348 (2.23 Å), glu197 (2.81 Å), and his438 (2.17 Å) at the active site of BChE, respectively. There are hydrogen bonds between complexes 1–3 and with thr199 (2.40 Å) and his200 (2.54 Å); gln92 (2.94 Å), his94 (3.02 Å), his200 (2.50 Å); and gln92 (2.89 Å) in the active site of CA I enzyme, respectively. There are hydrogen bonds between complexes 1–3 and with his94 (2.36 Å), his96 (2.62 Å), thr199 (2.21 Å), thr200 (2.41 Å), tyr7 (2.53 Å); thr199 (2.07 Å) and thr200 (2.41 Å); and gln92 (2.43 Å), thr199 (1.98 Å), thr200 (2.57 Å), and pro201 (3.01 Å) in the active site of CA II enzyme, respectively. Complex 1–3 form hydrogen bonds with ser51 (1.82 Å), glu50 (1.69 Å), gly158 (2.45 Å), and asp331 (2.60 Å); his52 (2.99 Å), thr57 (2.16 Å), and ala155 (2.84 Å); and asp227 (2.35 Å), ile367 (1.93 Å), gly381 (2.36 Å), and his434 (2.86 Å) amino acid residues at the active site of GR, respectively. When these hydrogen bonds were evaluated in general, it was determined that all complexes formed strong hydrogen bonds with the active sites of the target proteins. According to the results of

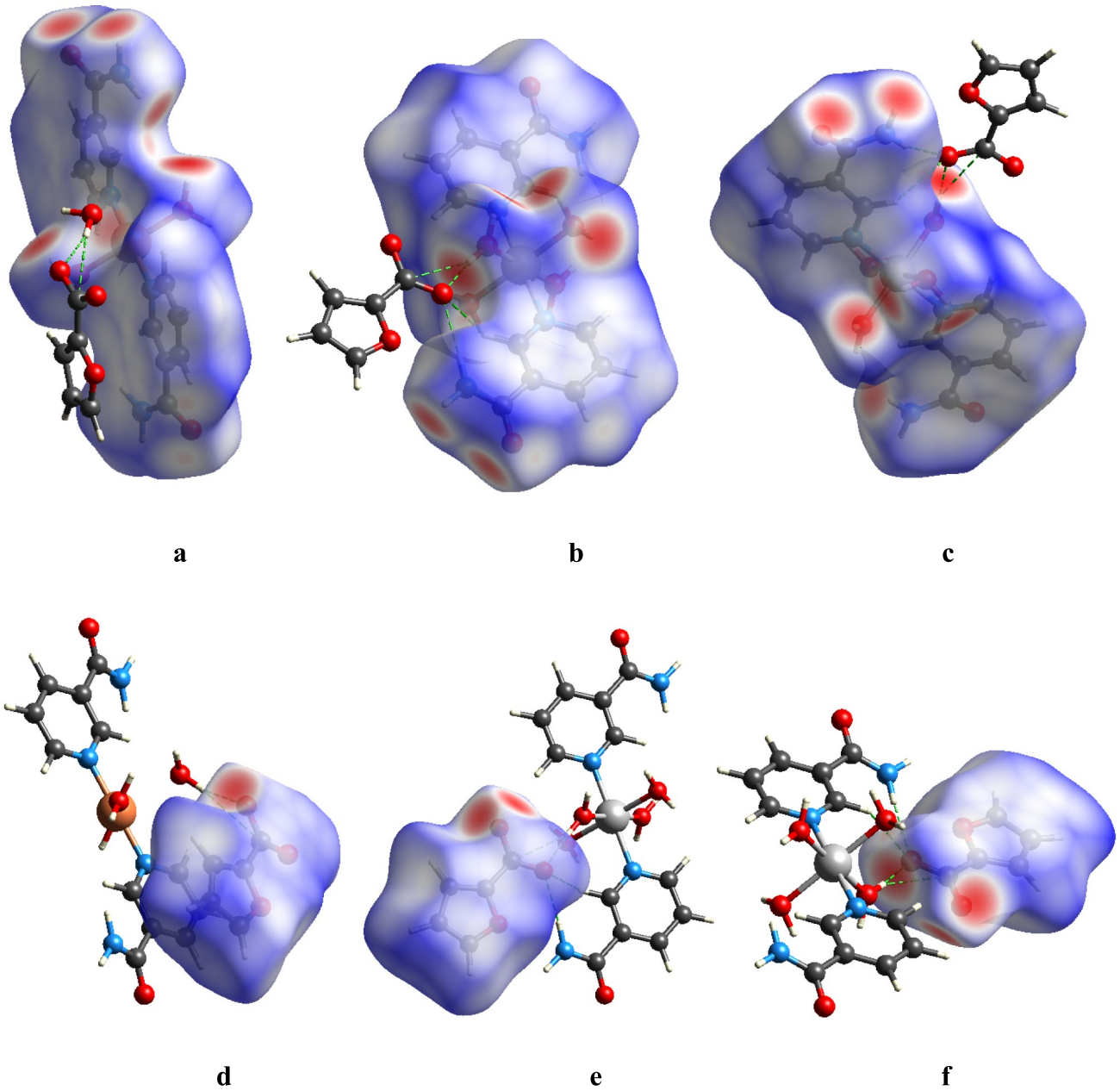


Fig. 4 D_{norm} map of cationic unit of Complex 1 (**a**), cationic unit of Complex 2 (**b**), and cationic unit of Complex 3 (**c**), anionic unit of Complex 1 (**d**), anionic unit of Complex 2 (**e**), and anionic unit of Complex 3 (**f**)

molecular docking studies, it is seen that Complex 2 may be an important agent in inhibiting target enzymes. 2D interactions between the synthesized complexes and the target enzymes are given in Fig. S14.

Correlation between in vitro and in silico results

A critical comparison of the *in vitro* enzyme inhibition results with the molecular docking study highlights a clear consistency between the two datasets. Complex 2 stands out as the most potent inhibitor across nearly all tested enzymes, showing the lowest K_i values (98.6 nM for hCA I, 68.0 nM for hCA II, and 7.5 nM for GR), and this trend is fully supported by its docking scores, which are the most favorable among the series (−10.7, −10.1, −8.2, −9.4, and −9.7 kcal/mol for AChE, BChE, hCA I, hCA II, and GR, respectively). The superior binding affinity of Complex 2 can be attributed to its ability to form multiple stable hydrogen bonds and π-type interactions with key residues within the enzyme active sites, as confirmed by the docking analysis.

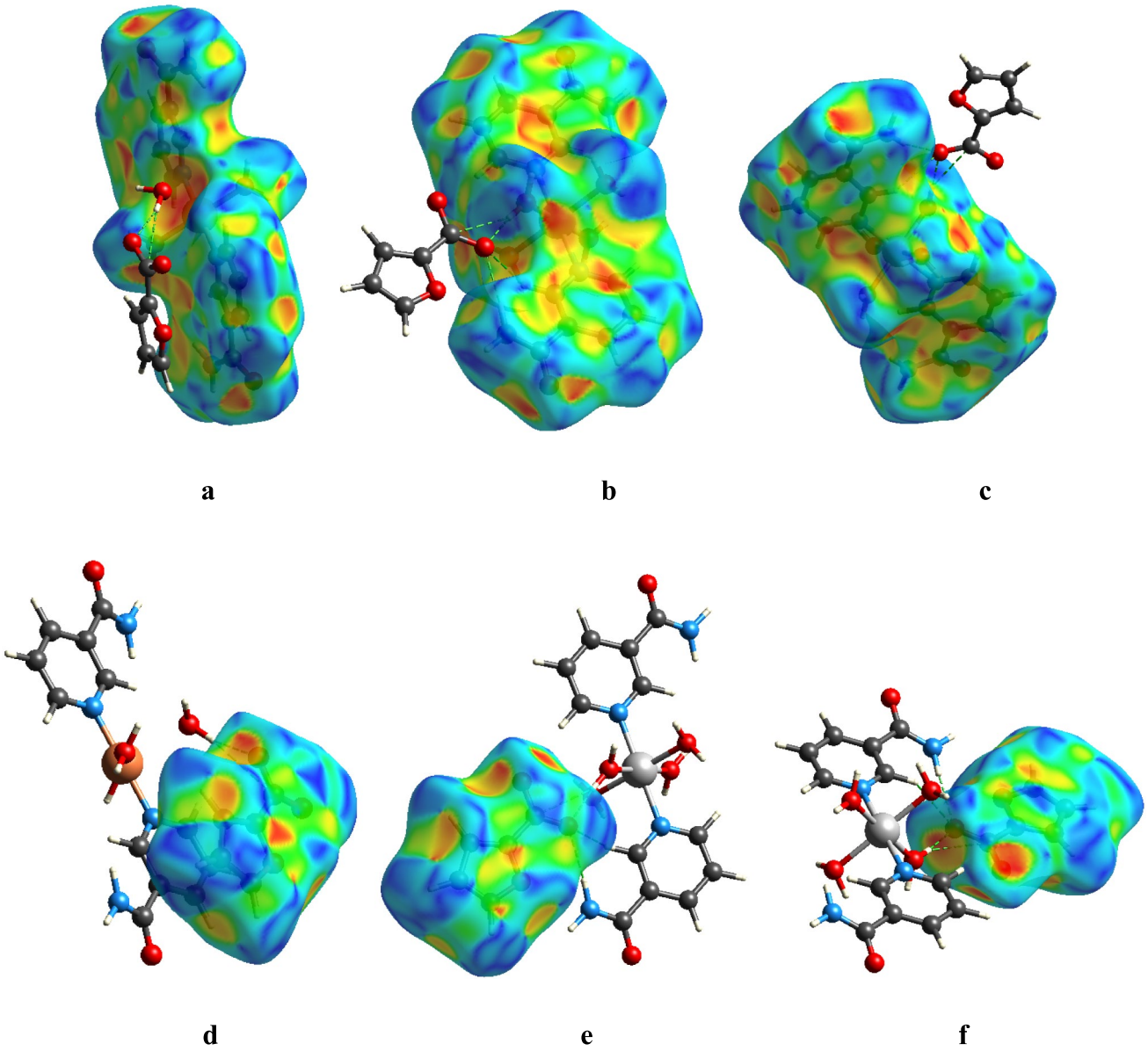


Fig. 5 The shape index of the cationic unit of Complex 1 (**a**), the cationic unit of Complex 2 (**b**), and the cationic unit of Complex 3 (**c**), the anionic unit of Complex 1 (**d**), the anionic unit of Complex 2 (**e**), and the anionic unit of Complex 3 (**f**)

Complex 1 displayed intermediate inhibitory activity, particularly against AChE ($K_i = 151.6$ nM) and BChE (234.8 nM), which correlates well with its moderately strong docking affinities (−9.4 and −9.9 kcal/mol, respectively). In contrast, Complex 3 consistently exhibited weaker inhibitory effects *in vitro* (e.g., $K_i = 257.4$ nM for AChE, 222.7 nM for hCA I, and 16.6 nM for GR), and this is reflected in its comparatively less favorable binding energies (−7.5 to −8.4 kcal/mol). Notably, for the CA enzymes, the order of inhibition (Complex 2 > Complex 1 > Complex 3) parallels the order of docking binding energies, reinforcing the predictive accuracy of the computational approach.

Overall, the agreement between experimental and computational results provides validation for the molecular docking methodology employed in this study. These correlations strengthen the structure–activity relationship analysis, support the reliability of docking-based predictions, and suggest that *in silico* modeling may be a valuable tool for guiding the design of future derivatives with enhanced enzyme inhibitory properties.

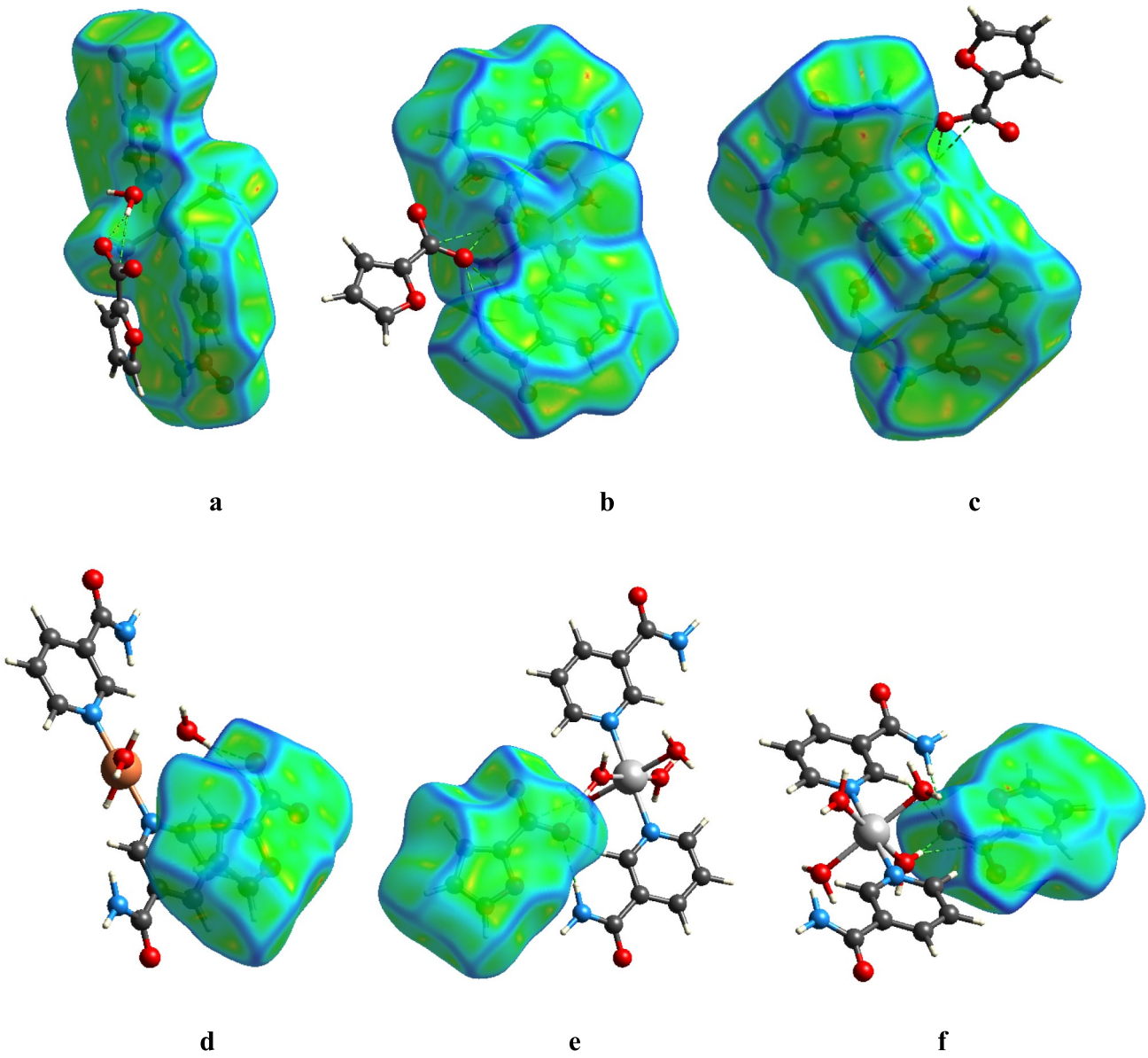


Fig. 6 The curvedness map of the cationic unit of Complex 1 (**a**), the cationic unit of Complex 2 (**b**), and the cationic unit of Complex 3 (**c**), the anionic unit of Complex 1 (**d**), the anionic unit of Complex 2 (**e**), and the anionic unit of Complex 3 (**f**)

ADMET properties

Predicting the pharmacokinetic and toxicokinetic properties of compounds with drug candidate potential increases the probability of success in drug development studies. Lipinski et al. reported five rules for assessing whether a compound would be a drug candidate [55]. The *in silico* drug-likeness and pharmacokinetic profiles of the synthesized complexes 1–3 were evaluated using the SwissADME tool (Table S3). All three compounds displayed comparable physicochemical properties with molecular weights around 375–382 g/mol, moderate polarity (TPSA = 132.96 $Å^2$), and similar molar refractivity (76.91). Their consensus Log P values (≈ –2.7) indicated hydrophilic character, which was consistent with the high solubility predictions. Indeed, all complexes were classified as "very soluble" according to ESOL and Ali models, while the SILICOS-IT model suggested solubility in the "soluble" range. Pharmacokinetic predictions revealed high gastrointestinal absorption for each complex, while none were permeable to the blood–brain barrier, suggesting their biological distribution may remain peripheral. Importantly, none of the complexes were predicted to act as substrates of P-glycoprotein or as inhibitors of the major cytochrome P450 isoenzymes (CYP1A2, CYP2C19, CYP2C9, CYP2D6,

Table 4 Percentages of intermolecular interactions according to 2D fingerprint graphs of complexes 1–3

	Complex 1		Complex 2		Complex 3	
	Cationic unit	Anionic unit	Cationic unit	Anionic unit	Cationic unit	Anionic unit
H…H	38.9	31.9	40.7	32.3	40.6	32.6
H…O/O…H	34.9	42.7	37.9	41.8	38.1	41.7
C…C	9.1	11.3	8.7	11.3	8.7	11.3
C…O/O…C	4.4	5.0	4.8	5.7	4.7	5.7
H…C/C…H	5.0	5.7	4.0	5.5	4.0	5.3
H…N/N…H	4.0	1.6	2.7	1.8	2.7	1.8
C…N/N…C	0.6	0.8	0.7	0.9	0.7	0.9
N…O/O…N	0.4	0.4	0.2	0.2	0.2	0.2
O…O	0.6	0.7	0.2	0.3	0.2	0.4
H…Cu/Cu…H	0.3	-	-	-	-	-
O…Cu/Cu…O	1.8	-	-	-	-	-

Table 5 IC_{50} values (nM) obtained with tested enzymes for complexes 1–3 and reference molecules

Inhibitor	AChE	BChE	hCA I	hCA II	GR
Complex 1 (Cu)	318.3 ± 4.7	528.4 ± 6.8	382.3 ± 3.9	387.5 ± 4.1	28.3 ± 0.32
Complex 2 (Co)	382.8 ± 4.3	703.8 ± 8.4	192.4 ± 2.5	156.6 ± 0.1.8	16.2 ± 0.17
Complex 3 (Zn)	553.4 ± 6.1	936.9 ± 9.8	467.7 ± 5.3	440.0 ± 4.7	31.6 ± 0.34
Donepezil	392.7 ± 42.1	2351.4 ± 241.2	-	-	-
NNS	-	-	-	-	645 μM

Table 6 K_i values (nM) obtained with tested enzymes for Complexes 1–3, reference molecules

Inhibitor	AChE	BChE	hCA I	hCA II	GR
Complex 1 (Cu)	151.6 ± 1.9	234.8 ± 4.1	201.2 ± 8.7	176.1 ± 5.1	13.5 ± 0.3
Complex 2 (Co)	184.0 ± 2.6	306.0 ± 6.7	98.6 ± 3.74	68.0 ± 2.5	7.5 ± 0.2
Complex 3 (Zn)	257.4 ± 3.2	425.9 ± 6.2	222.7 ± 9.1	195.5 ± 7.9	16.6 ± 0.4
Donepezil	201.4 ± 3.1	1022.3 ± 11.4	-	-	-
AZA	-	-	368 ± 8.7	34.6 ± 1.9	-

Errors within the range of 1–2% were observed in the presented data, as obtained from three distinct assays

CYP3A4), indicating a potentially favorable metabolism and low risk of drug–drug interactions. Skin permeation values (log Kp ≈ −9.5 cm/s) further confirmed limited transdermal absorption. Taken together, these findings demonstrate that all three complexes possess broadly comparable ADME and drug-likeness characteristics. Although their relatively high polarity and hydrogen bonding capacity may restrict passive membrane permeability, the favorable predictions regarding solubility, gastrointestinal absorption, and metabolic safety profile suggest that the complexes 1 and 2 in particular may represent promising scaffolds for further biological evaluation, whereas Complex 3 analogue requires additional consideration due to the heavy metal alert.

Complexes 1–3 are inactive in hepatotoxicity, carcinogenicity, immunotoxicity, mutagenicity, cytotoxicity, AMES toxicity, and mitochondrial membrane potential (MMP). The human Ether-a-go-go-Related Gene inhibition potential of the complexes was determined to be weak. Considering all these advantages and disadvantages, it is recommended to carry out further drug formulation studies to determine whether the complexes can be drug candidates.

Conclusions

The coordination compounds of Cu^{+2}, Co^{+2}, and Zn^{+2} cations were synthesized, and their structural characterizations were presented. Nicotinamide (N-donor) and aqua (O-donor) ligands with electron-donating groups were coordinated around the same metal. The structure of the Cu^{2+}, Co^{2+}, and Zn^{2+} complexes elucidated by single crystal structure analysis was found to have a distorted octahedral geometry with furan 2-carboxylic acid anions in the crystal structure coordinated by two nicotinamide and four water ligands. Cu^{2+}, Co^{2+}, and Zn^{2+} complexes were evaluated for their inhibitory activities against hCA isoforms (I,

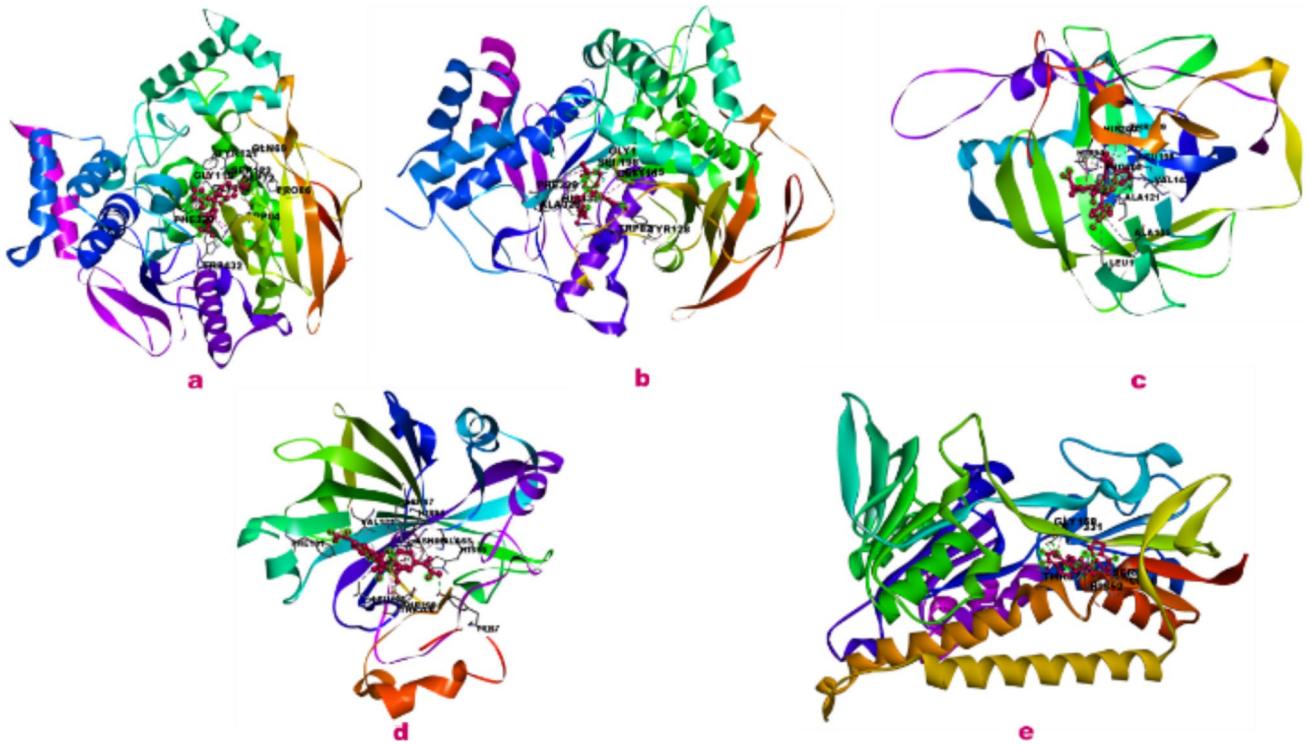


Fig. 7 3D representation of the docking of Complex 2 to the active site of the enzymes AChE (**a**), BChE (**b**), CA I (**c**), CA II (**d**), and GR (**e**)

II), cholinesterases (AChE, BChE), and GR. The results showed that the complexes exhibited potent inhibition at the nanomolar levels against these five enzymes. Interestingly, this study is also the first to report the inhibitory effects of these metal complexes on hCA I, II, and GR. Molecular docking studies further supported these findings, showing that Complex 2 had the highest binding affinity to all target enzymes, followed by Complex 1 and Complex 3. The docking studies revealed strong hydrogen bond interactions with key amino acid residues in the active sites of the enzymes, as well as π-π stacking and hydrophobic interactions, which contribute to the high inhibitory activity observed. Complex 2 exhibited the most favorable binding energy, with values of −10.7 kcal/mol for AChE, −10.1 kcal/mol for BChE, −8.2 kcal/mol for hCA I, −9.4 kcal/mol for hCA II, and −9.7 kcal/mol for GR, indicating its potential as a highly effective enzyme inhibitor. Additionally, ADMET (Absorption, Distribution, Metabolism, Excretion, and Toxicity) predictions provided valuable insights into the pharmacokinetic and toxicological properties of these metal complexes. The analysis indicated that all three complexes have low gastrointestinal absorption and do not cross the blood–brain barrier (BBB), suggesting that further formulation studies are needed to enhance their bioavailability. However, the complexes exhibited no significant hepatotoxicity, carcinogenicity, immunotoxicity, or mutagenicity risks, making them promising candidates for further pharmacological development. Overall, this study presents the first report on the enzyme inhibitory effects of Cu(II), Co(II), and Zn(II) furan-2-carboxylate nicotinamide complexes. The potent enzyme inhibition, particularly by the Co(II) complex, highlights their potential therapeutic applications in the treatment of diseases such as Alzheimer's disease, glaucoma, epilepsy, malaria, and cancer. Future studies should focus on optimizing their pharmacokinetic profiles and conducting detailed *in vivo* evaluations to further validate their therapeutic potential. Given their broad-spectrum inhibition, these metal complexes have the potential to be developed into promising agents for the treatment of various diseases, including glaucoma, epilepsy, malaria, and cancer.

Supplementary Information The online version contains supplementary material available at https://doi.org/10.1007/s11224-025-02625-0.

Author contribution Merve Nar: Writing – original draft, Methodology, Investigation, Conceptualization, Formal analysis, Data curation. Murat Şentürk: Writing – original draft, Visualization, Validation, Methodology, Investigation, Conceptualization. Afşin Ahmet Kaya: Writing – original draft, Visualization, Validation, Methodology, Investigation, Conceptualization, Supervision. Füreya Elif Öztürkkan: Writing – original draft, Methodology, Investigation, Software, Visualization. Elif Çelenk Kaya: Writing – original draft, Methodology, Investigation, Conceptualization, Resources. Ertan Şahin: Writing – original draft, Methodology, Investigation, Visualization, Conceptualization.

Funding The authors received no financial support or funding for the research, authorship, and/or publication of this article.

Data Availability All data generated or analyzed during this study are included in the supplementary material of this article. No additional data are available.

Declarations

Ethics approval This study did not involve any human participants or animal experiments. Therefore, ethical approval was not required.

Competing interests The authors declare no competing interests.

References

1. Supuran CT (2008) Carbonic anhydrases: novel therapeutic applications for inhibitors and activators. Nat Rev Drug Discov 7:168–181. https://doi.org/10.1038/nrd2467
2. Reitz C, Brayne C, Mayeux R (2011) Epidemiology of Alzheimer disease. Nat Rev Neurol 7:137–152. https://doi.org/10.1038/nrneurol.2011.2
3. Wang H, Zhang H (2019) Reconsideration of anticholinesterase therapeutic strategies against Alzheimer's disease. ACS Chem Neurosci 10:852–862. https://doi.org/10.1021/acschemneuro.8b00391
4. Aquilano K, Baldelli S, Ciriolo MR (2014) Glutathione: new roles in redox signaling for an old antioxidant. Front Pharmacol. https://doi.org/10.3389/fphar.2014.00196
5. Panek D, Więckowska A, Jończyk J, Godyń J, Bajda M, Wichur T, Pasieka A, Knez D, Pišlar A, Korabecny J, Soukup O, Sepsova V, Sabaté R, Kos J, Gobec S, Malawska B (2018) Design, synthesis, and biological evaluation of 1-benzylamino-2-hydroxyalkyl derivatives as new potential disease-modifying multifunctional anti-Alzheimer's agents. ACS Chem Neurosci 9:1074–1094. https://doi.org/10.1021/acschemneuro.7b00461
6. Is YS, Aksoydan B, Senturk M, Yurtsever M, Durdagi S (2020) Integrated binary QSAR-driven virtual screening and in vitro studies for finding novel hMAO-B-selective inhibitors. J Chem Inf Model 60:4047–4055. https://doi.org/10.1021/acs.jcim.0c00169
7. Kaya EÇ, Demircioğlu Z, Kaya AA, Büyükgüngör O (2015) Synthesis, X-ray structural, characterization, NLO, MEP, NBO, and HOMO–LUMO analysis using DFT study of Co(II)bis(3,4 dimethoxybenzoate)bis(nicotinamide) dihydrate. Mol Cryst Liq Cryst 609:103–117. https://doi.org/10.1080/15421406.2014.927964
8. Yaseen R, Ekinci D, Senturk M, Hameed ADh, Ovais S, Rathore P, Samim M, Javed K, Supuran CT (2016) Pyridazinone substituted benzenesulfonamides as potent carbonic anhydrase inhibitors. Bioorg Med Chem Lett 26:1337–1341. https://doi.org/10.1016/j.bmcl.2015.12.016
9. Özil M, Balaydın HT, Şentürk M (2019) Synthesis of 5-methyl-2,4-dihydro-3*H*-1,2,4-triazole-3-one's aryl Schiff base derivatives and investigation of carbonic anhydrase and cholinesterase (AChE, BuChE) inhibitory properties. Bioorg Chem 86:705–713. https://doi.org/10.1016/j.bioorg.2019.02.045
10. Sippel KH, Robbins AH, Domsic J, Genis C, Agbandje-McKenna M, McKenna R (2009) High-resolution structure of human carbonic anhydrase II complexed with acetazolamide reveals insights into inhibitor drug design. Acta Crystallogr Sect F Struct Biol Cryst Commun 65:992–995. https://doi.org/10.1107/S1744309109036665
11. Rocca WA, Petersen RC, Knopman DS, Hebert LE, Evans DA, Hall KS, Gao S, Unverzagt FW, Langa KM, Larson EB, White LR (2011) Trends in the incidence and prevalence of Alzheimer's disease, dementia, and cognitive impairment in the United States. Alzheimers Dement 7:80–93. https://doi.org/10.1016/j.jalz.2010.11.002
12. Arslan T, Buğrahan Ceylan M, Baş H, Biyiklioglu Z, Senturk M (2020) Design, synthesis, characterization of peripherally tetra-pyridine-triazole-substituted phthalocyanines and their inhibitory effects on cholinesterases (AChE/BChE) and carbonic anhydrases (hCA I, II and IX). Dalton Trans 49:203–209. https://doi.org/10.1039/C9DT03897C
13. Georges J, Jansen S, Jackson J, Meyrieux A, Sadowska A, Selmes M (2008) Alzheimer's disease in real life – the dementia carer's survey. Int J Geriatr Psychiatry 23:546–551. https://doi.org/10.1002/gps.1984
14. Sola I, Aso E, Frattini D, López-González I, Espargaró A, Sabaté R, Di Pietro O, Luque FJ, Clos MV, Ferrer I, Muñoz-Torrero D (2015) Novel levetiracetam derivatives that are effective against the Alzheimer-like phenotype in mice: synthesis, in vitro, ex vivo, and in vivo efficacy studies. J Med Chem 58(15):6018–6032. https://doi.org/10.1021/acs.j.medchem.5b00624
15. Arslan T, Çakır N, Keleş T, Biyiklioglu Z, Senturk M (2019) Triazole substituted metal-free, metallo-phthalocyanines and their water soluble derivatives as potential cholinesterases inhibitors: design, synthesis and in vitro inhibition study. Bioorg Chem 90:103100. https://doi.org/10.1016/j.bioorg.2019.103100
16. Song M-S, Matveychuk D, MacKenzie EM, Duchcherer M, Mousseau DD, Baker GB (2013) An update on amine oxidase inhibitors: multifaceted drugs. Prog Neuro-Psychopharmacol Biol Psychiatry 44:118–124. https://doi.org/10.1016/j.pnpbp.2013.02.001
17. Casey DA, Antimisiaris D, O'Brien J (2010) Drugs for Alzheimer's disease: are they effective? P T 35:208–211
18. Arslan T, Biyiklioglu Z, Şentürk M (2018) The synthesis of axially disubstituted silicon phthalocyanines, their quaternized derivatives and first inhibitory effect on human cytosolic carbonic anhydrase isozymes hCA I and II. RSC Adv 8:10172–10178. https://doi.org/10.1039/C7RA13674A
19. Işık S, Vullo D, Durdagi S, Ekinci D, Şentürk M, Çetin A, Şentürk E, Supuran CT (2015) Interaction of carbonic anhydrase isozymes I, II, and IX with some pyridine and phenol hydrazinecarbothioamide derivatives. Bioorg Med Chem Lett 25:5636–5641. https://doi.org/10.1016/j.bmcl.2015.10.021
20. Arslan T, Türkoğlu EA, Şentürk M, Supuran CT (2016) Synthesis and carbonic anhydrase inhibitory properties of novel chalcone substituted benzenesulfonamides. Bioorg Med Chem Lett 26:5867–5870. https://doi.org/10.1016/j.bmcl.2016.11.017
21. Güney M, Çavdar H, Şentürk M, Ekinci D (2015) Synthesis and carbonic anhydrase inhibitory properties of novel uracil derivatives. Bioorg Med Chem Lett 25:3261–3263. https://doi.org/10.1016/j.bmcl.2015.05.073
22. Korkmaz N, Obaidi OA, Senturk M, Astley D, Ekinci D, Supuran CT (2015) Synthesis and biological activity of novel thiourea derivatives as carbonic anhydrase inhibitors. J Enzyme Inhib Med Chem 30:75–80. https://doi.org/10.3109/14756366.2013.879656
23. Kocaoğlu E, Talaz O, Çavdar H, Şentürk M, Supuran CT, Ekinci D (2019) Determination of the inhibitory effects of N-methylpyrrole derivatives on glutathione reductase enzyme. J Enzyme Inhib Med Chem 34:51–54. https://doi.org/10.1080/14756366.2018.1520228
24. Krauth-Siegel RL, Bauer H, Schirmer RH (2005) Dithiol proteins as guardians of the intracellular redox milieu in parasites: old and new drug targets in trypanosomes and malaria-causing plasmodia. Angew Chem Int Ed 44:690–715. https://doi.org/10.1002/anie.200300639

25. Sumrra SH, Anees M, Asif A, Zafar MN, Mahmood K, Nazar MF, Khalid M, Nadeem MA, Khan MU (2020) Synthesis, structural, spectral and biological evaluation of metals endowed 1,2,4-triazole. Bull Chem Soc Eth 34:335–351. https://doi.org/10.4314/bcse.v34i2.11
26. Sumrra SH, Zafar W, Malik SA, Mahmood K, Shafqat SS, Arif S (2022) Metal based bioactive nitrogen and oxygen donor mono and bis Schiff bases: design, synthesis, spectral characterization, computational analysis and antibacterial screening. Acta Chim Slov 69:200–216. https://doi.org/10.17344/acsi.2021.7182
27. Sumrra SH, Ramzan S, Mustafa G, Ibrahim M, Mughal EU, Nadeem MA, Chohan ZH, Khalid M (2018) Complexes of imino-1,2,4-triazole derivative with transition metals: synthesis and antibacterial study. Russ J Gen Chem 88:1707–1711. https://doi.org/10.1134/S1070363218080248
28. Aydoğdu Ö, Öztürkkan FE, Hökelek T, Uğurlu G, Necefoğlu H (2025) Syntheses, crystal structures, and DFT calculations of N'-(pyridin-2-ylmethylene)nicotinohydrazide dihydrate and its copper complex. J Iran Chem Soc 22:683–697. https://doi.org/10.1007/s13738-025-03177-0
29. Köse DA, Kaya A, Necefoğlu H (2007) Synthesis and characterization of bis(N,N-diethylnicotinamide) m-hydroxybenzoate complexes of Co(II), Ni(H), Cu(II), and Zn(II). Russ J Coord Chem 33:422–427. https://doi.org/10.1134/S1070328407060073
30. Kaya AA, Demircioğlu Z, Kaya EÇ, Büyükgüngör O (2014) Synthesis, X-ray structural characterization, NLO, MEP, NBO and HOMO-LUMO analysis using DFT study of Zn(II)bis(3,4 dimethoxybenzoate)bis(nicotinamide) dihydrate. Heterocycl Commun 20:51–59. https://doi.org/10.1515/hc-2013-0160
31. Sheldrick GM (2015) Crystal structure refinement with *SHELXL*. Acta Crystallogr C Struct Chem 71:3–8. https://doi.org/10.1107/S2053229614024218
32. Hirshfeld FL (1977) Bonded-atom fragments for describing molecular charge densities. Theor Chim Acta 44:129–138. https://doi.org/10.1007/BF00549096
33. Spackman MA, Jayatilaka D (2009) Hirshfeld surface analysis. CrystEngComm 11:19–32. https://doi.org/10.1039/B818330A
34. Spackman PR, Turner MJ, McKinnon JJ, Wolff SK, Grimwood DJ, Jayatilaka D, Spackman MA (2021) *Crystalexplorer* : a program for Hirshfeld surface analysis, visualization and quantitative analysis of molecular crystals. J Appl Crystallogr 54:1006–1011. https://doi.org/10.1107/S1600576721002910
35. McKinnon JJ, Jayatilaka D, Spackman MA (2007) Towards quantitative analysis of intermolecular interactions with Hirshfeld surfaces. Chem Commun 3814:3814. https://doi.org/10.1039/b704980c
36. Spackman MA, McKinnon JJ (2002) Fingerprinting intermolecular interactions in molecular crystals. CrystEngComm 4:378–392. https://doi.org/10.1039/B203191B
37. Noreen S, Sumrra SH, Chohan ZH, Mustafa G, Imran M (2023) Synthesis, characterization, molecular docking and network pharmacology of bioactive metallic sulfonamide-isatin ligands against promising drug targets. J Mol Struct 1277:134780. https://doi.org/10.1016/j.molstruc.2022.134780
38. Mustafa G, Sabir S, Sumrra SH, Zafar W, Arshad MN, Hassan AU, Akhtar A, Ashfaq M, Asiri AM (2025) Synthesis, structure elucidation, SC-XRD/DFT, molecular modelling simulations and DNA binding studies of 3,5-diphenyl-4,5-dihydro-1 *H* -pyrazole chalcones. J Biomol Struct Dyn 43:1831–1846. https://doi.org/10.1080/07391102.2023.2293260
39. Harel M, Schalk I, Ehret-Sabatier L, Bouet F, Goeldner M, Hirth C, Axelsen PH, Silman I, Sussman JL (1993) Quaternary ligand binding to aromatic residues in the active-site gorge of acetylcholinesterase. Proc Natl Acad Sci U S A 90:9031–9035. https://doi.org/10.1073/pnas.90.19.9031
40. Nachon F, Carletti E, Ronco C, Trovaslet M, Nicolet Y, Jean L, Renard P-Y (2013) Crystal structures of human cholinesterases in complex with huprine W and tacrine: elements of specificity for anti-Alzheimer's drugs targeting acetyl- and butyryl-cholinesterase. Biochem J 453:393–399. https://doi.org/10.1042/BJ20130013
41. Chakravarty S, Kannan KK (1994) Drug-protein interactions. Refined structures of three sulfonamide drug complexes of human carbonic anhydrase I enzyme. J Mol Biol 243:298–309. https://doi.org/10.1006/jmbi.1994.1655
42. Savvides SN, Karplus PA (1996) Kinetics and crystallographic analysis of human glutathione reductase in complex with a xanthene inhibitor (*). J Biol Chem 271:8101–8107. https://doi.org/10.1074/jbc.271.14.8101
43. Trott O, Olson AJ (2010) Autodock vina: improving the speed and accuracy of docking with a new scoring function, efficient optimization, and multithreading. J Comput Chem 31:455–461. https://doi.org/10.1002/jcc.21334
44. BIOVIA (2021) Dassault Systèmes, BIOVIA Discovery Studio Visualizer 2021, v21.1.0.20298. Dassault Systèmes, San Diego
45. Daina A, Michielin O, Zoete V (2017) Swissadme: a free web tool to evaluate pharmacokinetics, drug-likeness and medicinal chemistry friendliness of small molecules. Sci Rep 7:42717. https://doi.org/10.1038/srep42717
46. Banerjee P, Eckert AO, Schrey AK, Preissner R (2018) ProTox-II: a webserver for the prediction of toxicity of chemicals. Nucleic Acids Res 46:W257–W263. https://doi.org/10.1093/nar/gky318
47. Cheng F, Li W, Zhou Y, Shen J, Wu Z, Liu G, Lee PW, Tang Y (2012) AdmetSAR: a comprehensive source and free tool for assessment of chemical ADMET properties. J Chem Inf Model 52:3099–3105. https://doi.org/10.1021/ci300367a
48. Özbek FE, Tercan B, Şahin E, Necefoğlu H, Hökelek T (2009) Tetraaquabis(nicotinamide-κ N^1)cobalt(II) bis(2-fluorobenzoate). Acta Crystallogr E Struct Rep Online 65:m341–m342. https://doi.org/10.1107/S1600536809006771
49. Zeng M-H, Zhu L-H, Liang H, Ng SW (2006) Tetraaquabis(3-pyridinecarboxamide-κN)copper(II) bis(2,4,6-trinitrophenolate). Acta Crystallogr Sect E Struct Rep Online 62:m822–m823. https://doi.org/10.1107/S1600536806009500
50. Zaman IG, ÇaylakDelibaş N, Necefoğlu H, Hökelek T (2013) trans -Tetraaquabis(isonicotinamide-κ N1)zinc bis(3-hydroxybenzoate) tetrahydrate. Acta Crystallogr E Struct Rep Online 69:m198–m199. https://doi.org/10.1107/S1600536813006466
51. Bellamy LJ (1980) The infrared spectra of complex molecules: volume two advances in infrared group frequencies. Springer, Netherlands
52. Verpoorte JA, Mehta S, Edsall JT (1967) Esterase activities of human carbonic anhydrases B and C. J Biol Chem 242:4221–4229. https://doi.org/10.1016/S0021-9258(18)95800-X
53. Ellman GL, Courtney KD, Andres V, Featherstone RM (1961) A new and rapid colorimetric determination of acetylcholinesterase activity. Biochem Pharmacol 7:88–95. https://doi.org/10.1016/0006-2952(61)90145-9
54. Beutler E (1984) Red cell metabolism: a manual of biochemical methods, 3rd edn. Grune & Stratton, Orlando, FL
55. Lipinski CA, Lombardo F, Dominy BW, Feeney PJ (1997) Experimental and computational approaches to estimate solubility and permeability in drug discovery and development settings. Adv Drug Deliv Rev 23:3–25. https://doi.org/10.1016/S0169-409X(96)00423-1

Publisher's Note Springer Nature remains neutral with regard to jurisdictional claims in published maps and institutional affiliations.

Springer Nature or its licensor (e.g. a society or other partner) holds exclusive rights to this article under a publishing agreement with the author(s) or other rightsholder(s); author self-archiving of the accepted manuscript version of this article is solely governed by the terms of such publishing agreement and applicable law.